Supporting Information

Design of a Versatile Interconnecting Layer for Highly Efficient Series-Connected Polymer Tandem Solar Cells

Lijian Zuo,[a,b] Chih-Yu Chang,[b,c] Chu-Chen Chueh,[b] Shuhua Zhang,[a] Hanying Li,[a] Alex K.-Y. Jen[a,b*], and Hongzheng Chen[a*]

[a] State Key Laboratory of Silicon Materials, MOE Key Laboratory of Macromolecular Synthesis and Functionalization, Department of Polymer Science & Engineering, Zhejiang University, Hangzhou 310027, China, E-mail: hzchen@zju.edu.cn or ajen@uw.edu
[b] Department of Materials Science and Engineering, University of Washington, Seattle, WA 98195, USA, E-mail: ajen@uw.edu
[c] Department of Materials Science and Engineering, Feng Chia University, Taichung, Taiwan, China.

Materials and Equipment: The PTB7 and $PC_{71}BM$ were purchased from 1-materials Corp. and used as received. The PIDT-PhanQ was made by using the procedures described.[33] UV-visible absorption and transmittance spectra were measured on a Varian CARY100 Bio spectrophotometer. The XPS was measured in an integrated ultrahigh vacuum system equipped with multi-technique surface analysis system (Thermo ESCALAB 250Xi). AFM measurement was carried out on a multi-mode scanning probe microscope (Veeco) in tapping mode. The sheet resistance of ultra-thin Ag was measured by the four-point probes method.

Device Fabrication of Inverted devices: ITO glass substrates were cleaned by detergent, acetone, and isopropanol in ultra-sonic bath. Following the ultra-violet-Ozone treatment, the ZnO[34] films were deposited by spin-coating and annealed in air. Subsequently, the PIDT-PhanQ:$PC_{71}BM$ (from the solution of 20 mg/ml PIDT-PhanQ:$PC_{71}BM$=1:3 wt%, *o*-Dichlorobenzene (DCB):1-chloronaphthalene (CN)=100:3, vol%) or the PTB7:$PC_{71}BM$ (from the solution of 25 mg/ml PTB7:$PC_{71}BM$=1:1.5 wt%, chlorobenzene (CB):1,8-diiodeoctrane (DIO)=100:3, vol%) films were deposited by spin-coating. For the PIDT-

PhanQ based solar cells, after annealed for 5 min at 120 °C, the substrates were successively deposited MoO_3 (10 nm) and Ag (100 nm) by thermal evaporation to complete the front cells. For the PTB7 solar cells, the casted films were directly transferred into the vacuum chamber to deposit MoO_3 (10 nm) and Ag (100 nm).

Top-illuminated micro-cavity solar cells: The glass substrate was cleaned as the procedures for glass/ITO substrates. 100 nm patterned Ag was deposited on the glass, followed by the deposition of 20 nm ZnO. After that, 80 nm PTB7 was deposited and then transferred into the vacuum chamber to deposit a 10 nm thick MoO_3 as the interfacial layer, a 12 nm thick Ag as the transparent conductive electrode, and a 10 nm thick MoO_3 as the capping layer.

*Semitransparent solar cells***:** The procedures were exactly the same as that for the above mentioned inverted solar cells based on PIDT-PhanQ:$PC_{71}BM$, except that the thickness of the back Ag electrode was 12 nm.

Tandem solar cells: The tandem devices based on an inverted structure were fabricated as follow: ITO glass substrates were cleaned by detergent, acetone, and isopropanol in ultra-sonic bath. Following the ultra-violet-Ozone treatment, the ZnO films were deposited by spin-coating and annealed in air. Subsequently, the PIDT-PhanQ films were spin-coated. After annealing for 5 min at 120 °C, the substrates with PIDT-PhanQ film were successively deposited 10 nm thick MoO_3 and 0-14 nm thick Ag by thermal evaporation to complete the front cells. An ultra-thin PFN film of 10 nm was deposited to lower the work function of Ag, followed by casting PTB7:$PC_{71}BM$ to form back cells. Finally, the substrates were transferred into the vacuum chamber again to deposit MoO_3 (10 nm) and Ag (100 nm) to finish the device fabrication procedures.

Device Measurement: PCE values were determined from *J–V* curve measurements (using a Keithley 2400 source meter) under a 1 sun, AM 1.5G spectrum from a solar simulator with intensity calibrated by a standard silicon diode, which was calibrated at National Renewable Energy Lab (NREL). To accurately measure the device, the device area was defined by a 2·2 mm^2 aperture. External quantum efficiency spectra were measured based on a monochromator, chopper, lock-in amplifier, and light source.

Optical Simulation: Optical simulations based on the transfer matrix formalism (TMF)[31] were used to calculate the interference of reflected and transmitted light at each interface within the stratified devices. All the simulations are based on the assumptions of planar interfaces and total isotropy for all layers. However, the interference within the glass substrates is ignored because their thicknesses (2 mm) are much higher than the wavelengths of the simulated incident beams. In addition, 100% internal quantum efficiency and the AM1.5 intensity spectrum (ASTM G173-03) are assumed to calculate the theoretically maximum photocurrent density.

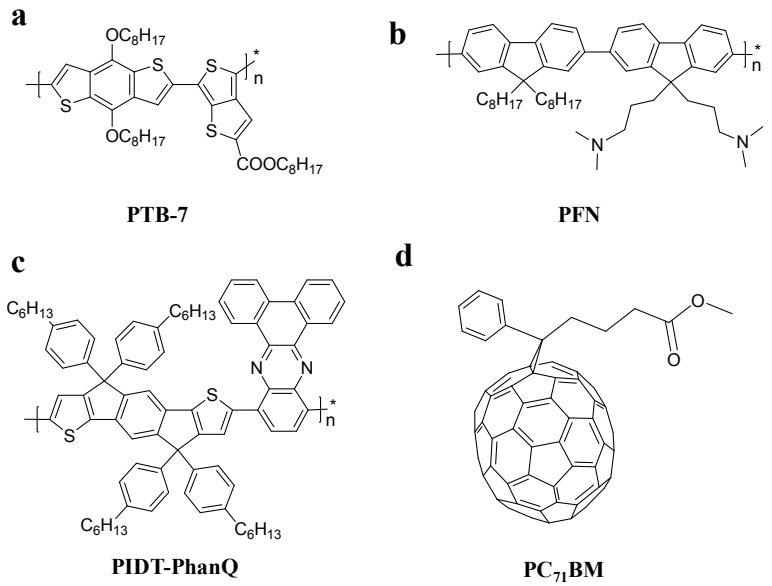

Figure S1. Chemical structures of (a) PTB7, (b) PFN, (c) PIDT-PhanQ, and (d) $PC_{71}BM$ used in this work.

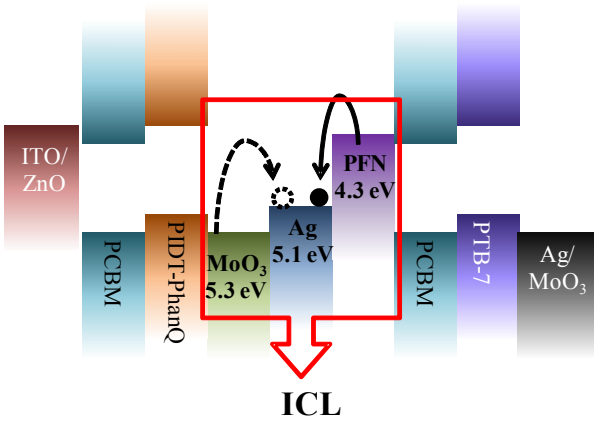

Figure S2. Schematic diagram of energy levels of each layer in polymer tandem solar cell. The interconnecting layer (MoO_3/Ag/PFN) would collect holes from the PIDT-PhanQ:$PC_{71}BM$ front sub-cell efficiently due to the high work function surface created by the MoO_3 layer, and would collect electrons from the PTB7:$PC_{71}BM$ back sub-cell efficiently due to the low work function surface created by the PFN layer. The collected charges would be efficiently recombined in the intermediate conducting ultra-thin Ag layer in ICL.

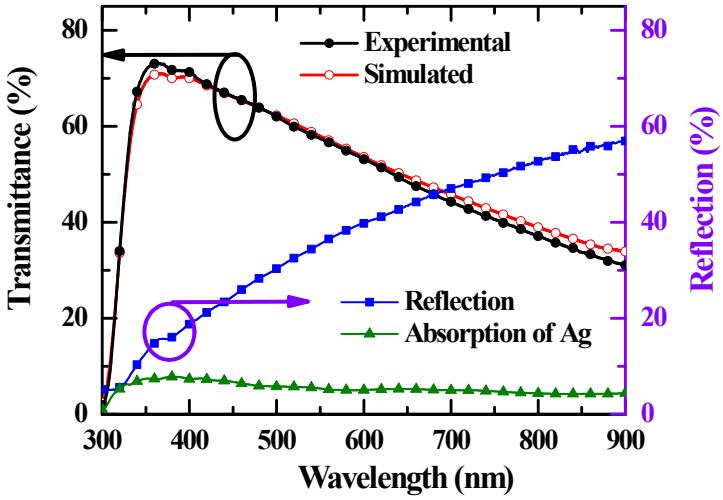

Figure S3. Transmittance (experimental result: open circle, simulated result: filled circle) of glass/Ag (12 nm), simulated reflectance (square) of glass/Ag (12 nm), and simulated parasitic absorption of 12 nm Ag in the structure of glass/Ag.

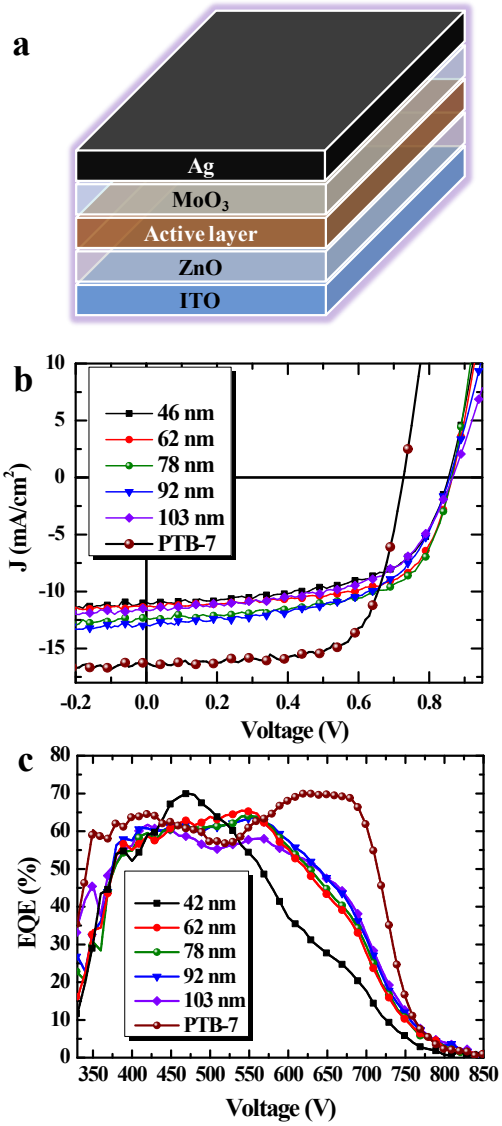

Figure S4. Inverted single junction solar cell device: (a) schematic diagram (ITO/ZnO/PIDT-PhanQ:$PC_{71}BM$ or PTB7:$PC_{71}BM$/MoO_3/Ag); *J-V* characteristics (b) and EQE spectra (c) of the PIDT-PhanQ:$PC_{71}BM$ based inverted single junction devices with different active layer thicknesses. The dark red curve is the in (b) and (c) is the *J-V* curve and EQE spectrum of PTB7:$PC_{71}BM$ based inverted solar cells with the same structure shown in (a), and the PTB7:$PC_{71}BM$ layer thickness is 82 nm.

Table S1. Device performance of PIDT-PhanQ:$PC_{71}BM$ based inverted single junction devices with different active layer thicknesses (d)

d of active layer	J_{SC}	V_{OC}	FF	PCE
(nm)	mA/cm^2	V		%
46	11.6	0.85	0.64	6.30
62	12.3	0.86	0.63	6.71
78	12.5	0.86	0.60	6.42
92	11.6	0.86	0.57	5.71
103	11.6	0.87	0.55	5.58

Table S2. Device performance of single junction devices based on PIDT-PhanQ:$PC_{71}BM$ and PTB7:$PC_{71}BM$ active layers

Active layer	Device structures	Transmittance AVT(%)	J_{SC}	V_{OC}	FF	PCE
			mA/cm^2	V		%
PIDT-PhanQ: $PC_{71}BM$	A	Opaque	12.30	0.86	0.63	6.71
	B	~ 25%	9.42	0.86	0.63	5.14
PTB7: $PC_{71}BM$	A	Opaque	16.22	0.73	0.69	8.22
	C	Opaque	15.25	0.73	0.73	8.17

Device structures: A, inverted device (ITO/ZnO/active layer/MoO_3(10 nm)/Ag(100 nm)); B, semitransparent device (ITO/ZnO/active layer/MoO_3(10 nm)/Ag(12 nm)); C, top-illuminated micro-cavity device (Ag/PFN/active layer/MoO_3(10 nm)/Ag(12 nm)/MoO_3(10 nm)).

Direct observation of micro-cavity formation in the ultra-thin Ag based organic solar cells:

The formation of micro-cavity in sub-cell is the essence of this work. However, the intrinsic absorption of the PTB7:$PC_{71}BM$ disturbed the direction observation of the micro-cavity based on the optimal device condition. Here, we purposely redistributed the micro-cavity center beyond the absorption region of the PTB7:$PC_{71}BM$ layer by increasing the active layer thickness to confirm the formation of micro-cavity effect in our designed devices. As shown in **Figure S5a**, the reflectance spectra of the ITO based devices show insignificant variation as the thickness of PTB7:$PC_{71}BM$ BHJ layer increases and the reflectance of the wavelength beyond the absorption region of PTB7:$PC_{71}BM$ (>700 nm) is very high. However, the reflection spectra of the ultra-thin Ag based devices show distinct drop in the region beyond the absorption of PTB7:$PC_{71}BM$ film. This reflectance valley formed in the ultra-thin Ag based devices is a direct evidence for the formation of micro-cavity effect in the device chamber. Moreover, the reflection valleys are gradually red-shifted while the thickness of the BHJ layer increases from 110 to 145 nm. The similar micro-cavity effect is also observed in the proposed tandem devices (**Figure S5c**), where the micro-cavity induced reflection valleys appear in the reflectance spectra beyond the absorption of the BHJ layers as well. This result clearly verifies the formation of micro-cavity in the ultra-thin Ag based devices.

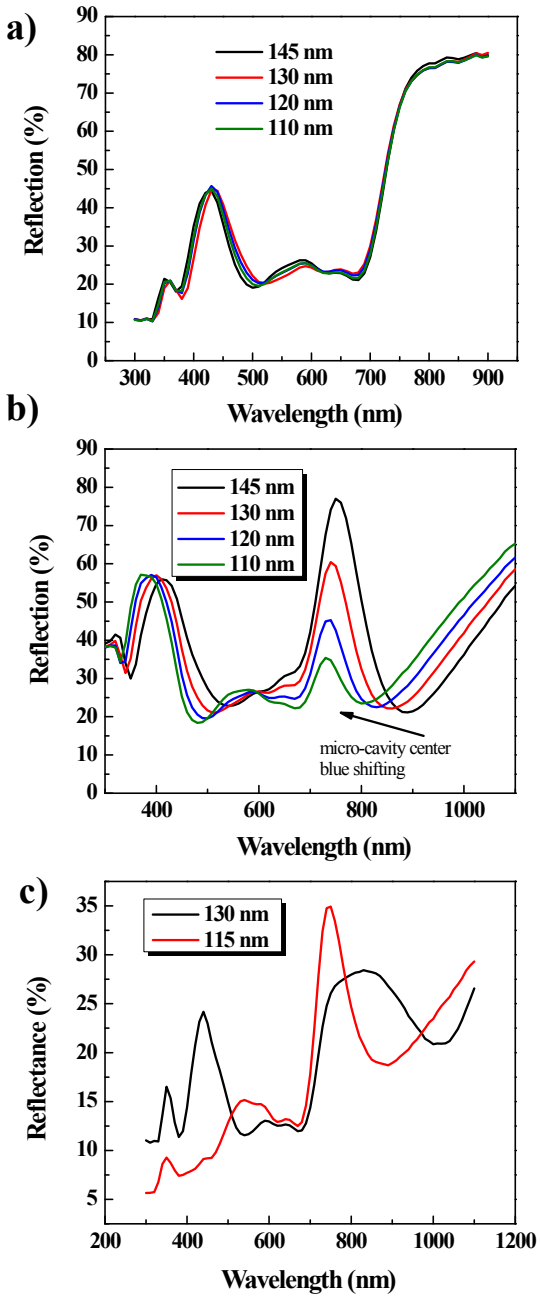

Figure S5. Reflectance spectra of ITO-based devices with different BHJ layer thicknesses (a), ultra-thin Ag based devices with different BHJ layer thicknesses (b) and the tandem devices with 115 and 130 nm PTB7:$PC_{71}BM$ BHJ layers (c).

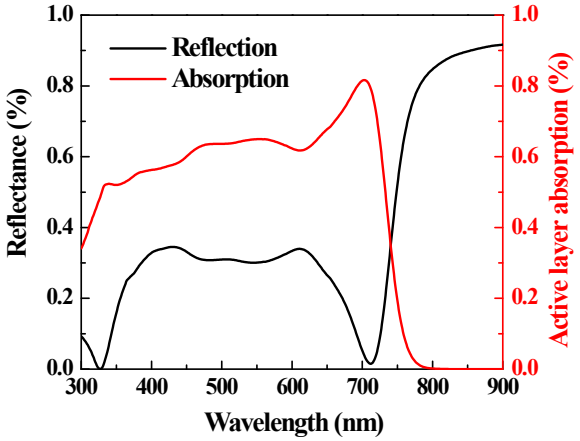

Figure S6. Simulated reflectance spectra and active layer absorption spectra of the micro-cavity device.

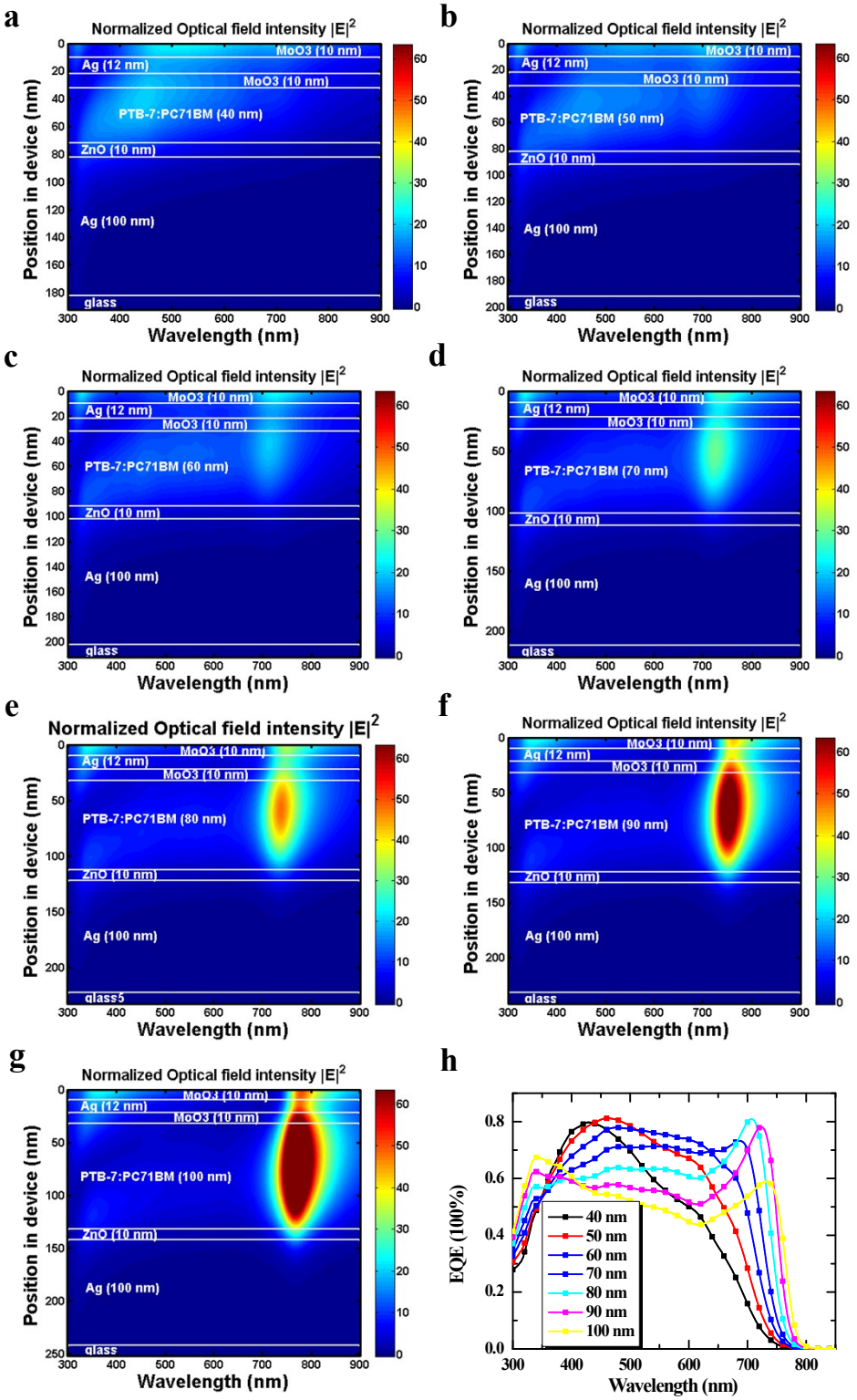

Figure S7. Simulation of the active layer thickness dependent optical field distributions (**a.** 40 nm, **b.** 50 nm, **c.** 60 nm, **d.** 70 nm, **e.** 80 nm, **f.** 90 nm, **g.** 100 nm) and the EQE (**h**) spectra of the top-illuminated devices with the micro-cavity structure: glass/Ag/ZnO/PTB7:$PC_{71}BM$/MoO_3/Ag/MoO_3.

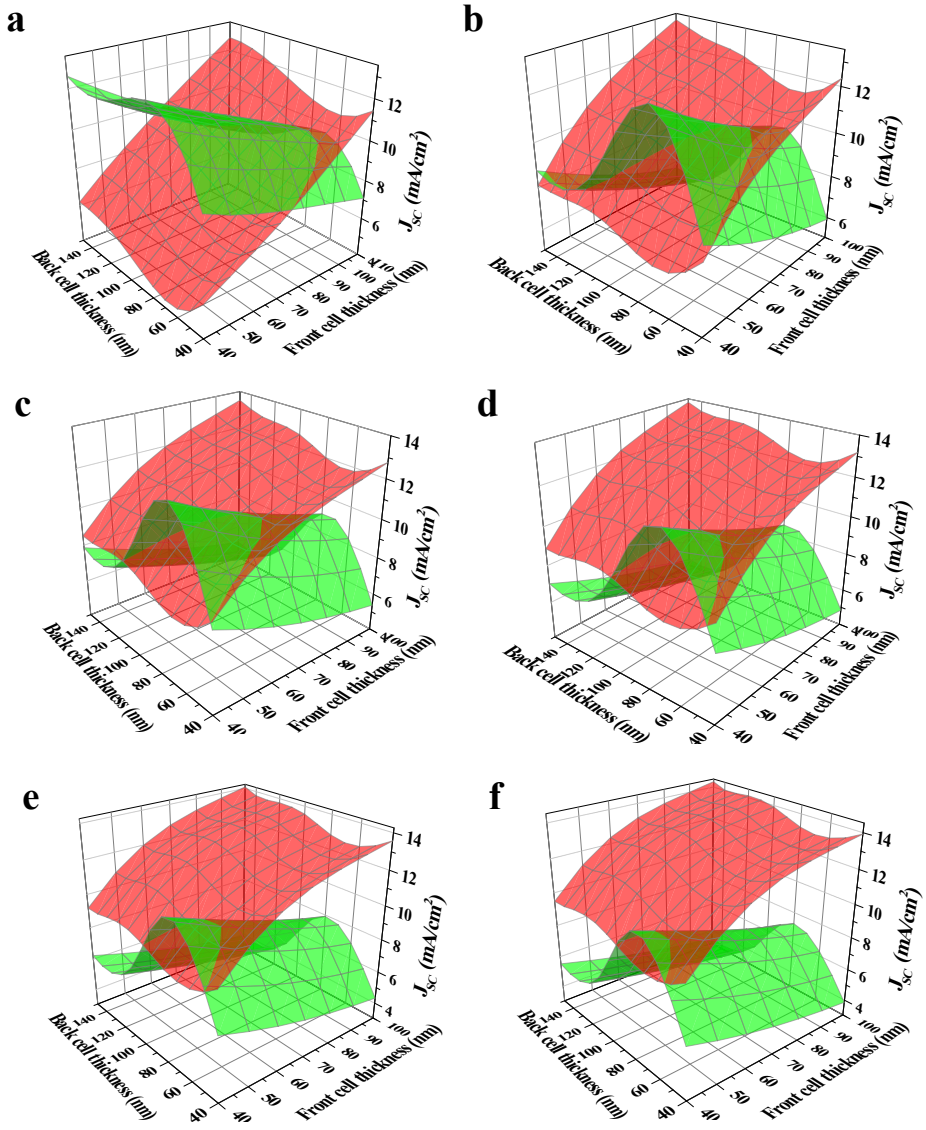

Figure S8. Simulation of the active layer thickness dependent J_{SC} in front and back sub-cells with different thicknesses of the ultra-thin Ag in the ICLs (device structure: glass/ITO/ZnO/PIDT-PhanQ:$PC_{71}BM$/MoO_3/Ag(0-16nm)/PFP/PTB7:$PC_{71}BM$/ MoO_3/Ag): **a.** 0 nm, **b.** 8 nm, **c.** 10 nm, **d.** 12 nm, **e.** 14 nm, **f.** 16 nm.

Table S3. Simulated Maximum achievable J_{SC} of sub-cells and the corresponding active layer thicknesses with different thicknesses of ultra-thin Ag films in ICLs.

Thickness of Ag (nm)	J_{SC} (mA/cm^2)		Active layer thickness (nm)	
ICLs	Front cell	Back cell	Front cell	Back cell
0	9.84	10.04	100	75
8	10.45	10.51	80	75
10	10.53	10.58	70	80
12	10.64	10.58	60	80
14	10.02	10.60	50	80
16	10.44	9.88	50	80

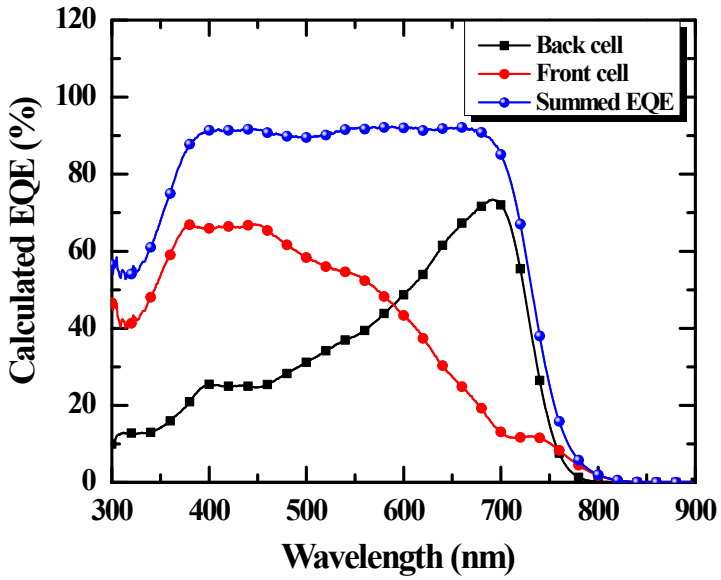

Figure S9. Simulated EQE spectra of the front and back sub-cells, assuming the IQE is 100% (device structure: glass/ITO/ZnO/PIDT-PhanQ:$PC_{71}BM$ (60 nm)/MoO_3/Ag (12 nm)/PFP/PTB7:$PC_{71}BM$ (80 nm)/MoO_3/Ag).

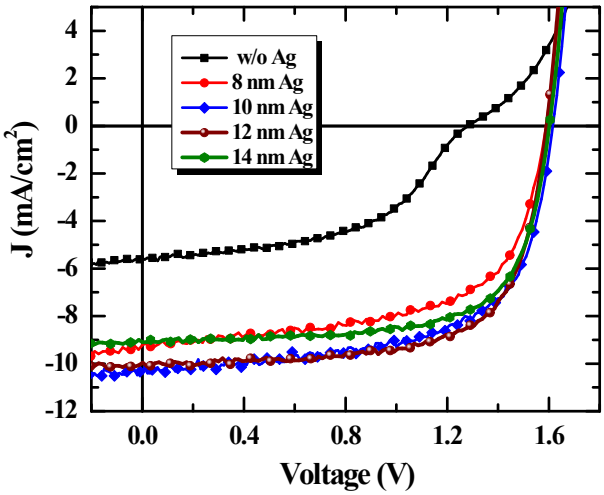

Figure S10. Ultra-thin Ag layer thickness dependent I-V characteristics of tandem devices with the structure: glass/ITO/ZnO/PIDT-PhanQ:$PC_{71}BM$ (60 nm)/MoO_3/Ag (0, 8, 10, 12, 14 nm)/PFP/PTB7:$PC_{71}BM$ (80 nm)/MoO_3/Ag).
\

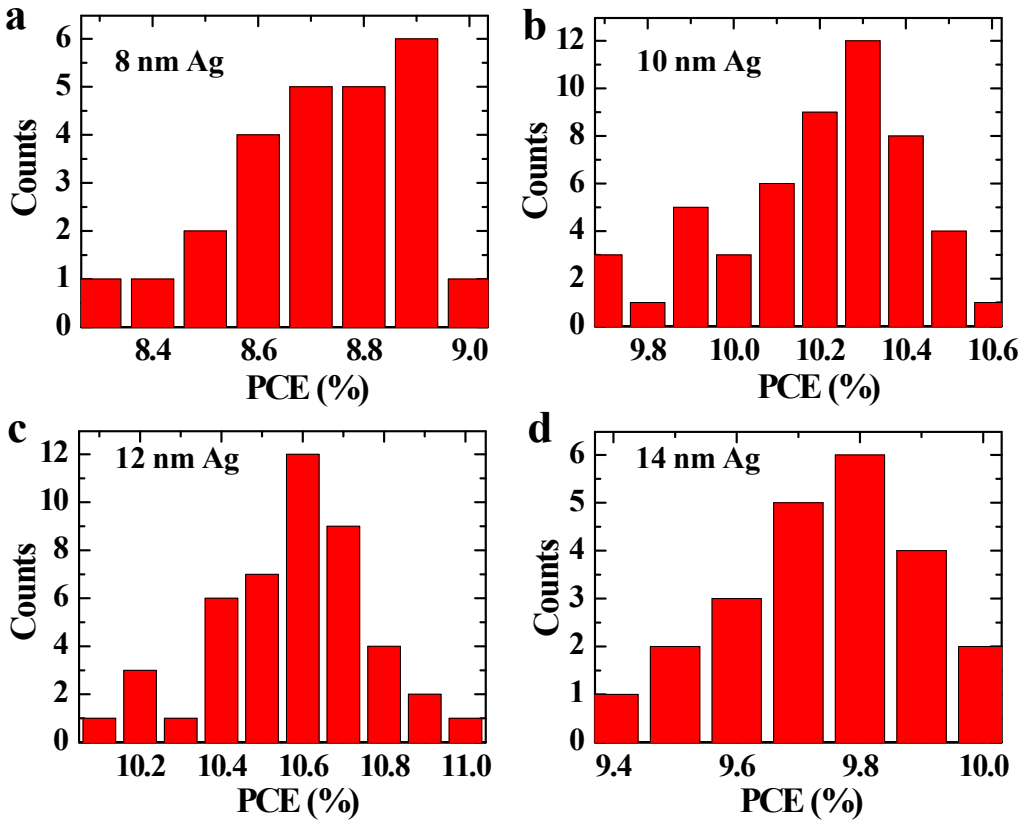

Figure S11. Histrogram of organic tandem solar cells efficiency with different thicknesses of Ag film in ICLs, device structure: glass/ITO/ZnO/PIDT-PhanQ:$PC_{71}BM$ (60 nm)/MoO_3/Ag (8, 10, 12, 14 nm)/PFP/PTB7:$PC_{71}BM$ (80 nm)/MoO_3/Ag), **a.** 8 nm Ag, **b.** 10 nm Ag, **c.** 12 nm Ag, **d.** 14 nm Ag. The device efficiency was summarized from more than 300 devices.